Magnetic structure, magnetic interactions and metamagnetism in terbium iron borate TbFe$_3$(BO$_3$)$_4$: a neutron diffraction and magnetization study

To cite this article: C Ritter *et al* 2007 *J. Phys.: Condens. Matter* **19** 196227

View the article online for updates and enhancements.

Magnetic structure, magnetic interactions and metamagnetism in terbium iron borate $TbFe_3(BO_3)_4$: a neutron diffraction and magnetization study

C Ritter[1], A Balaev[2], A Vorotynov[2], G Petrakovskiĭ[2], D Velikanov[2], V Temerov[2] and I Gudim[2]

[1] Institute Laue-Langevin, Boite Postale 156, F-38042 Grenoble, France
[2] L V Kirenskiĭ Institute of Physics, Siberian Branch of RAS, Krasnoyarsk, 660036, Russia

Abstract

Magnetization, susceptibility and neutron scattering measurements were performed on the terbium iron borate $TbFe_3(BO_3)_4$. Structural and magnetic phase transitions were obtained as a function of external magnetic field and temperature. A metamagnetic transition of the terbium spins and a spin-flop transition of the iron sublattice are obtained at an external magnetic field 35 kOe $< H_t <$ 60 kOe. The values of the effective exchange H_E and the anisotropy H_A fields are evaluated. Temperature dependent neutron diffraction studies reveal the magnetic structure of $TbFe_3(BO_3)_4$ and the thermal evolution of the two magnetic sublattices. An antiferromagnetic coupling along the helicoidal chains of Fe atoms sets in at 40 K with a propagation vector $k = [0\ 0\ \frac{1}{2}]$. The magnetic ordering of the Tb sublattice sets in at the same temperature and leads to an anti-parallel alignment of the Fe and Tb moments within the a–b-planes with $\mu_{Fe} = 4.4\ \mu_B$ and $\mu_{Tb} = 8.6\ \mu_B$ at 2 K.

(Some figures in this article are in colour only in the electronic version)

1. Introduction

Borates of general formula $RM_3(BO_3)_4$ with R being a rare earth and M = Al, Ga, Sc, Cr, Fe have recently been studied intensively due to the interesting optical properties shown by the Al compounds and the expected interesting magnetoelectric properties of the iron borates [1, 2]. Crystallizing in the space group $R32$ [3], the absence of an inversion centre is responsible for the good optoelectronic properties while the simultaneous presence of magnetic 3d ions and 4f ions should lead to a variety of magnetic interactions. The crystal structure of these borates is strongly anisotropic, as the M sublattice sees helicoidal chains of M^{3+} ions running along the c-axis. The distance between M^{3+} ions along these chains is significantly smaller than the distance between the chains, leading to some kind of one-dimensional structure element. At the

same time the rare earth ions are well isolated from each other, located in trigonal prisms RO_6 with no direct R–O–R links. A detailed description and a picture of the structure can be found in Campa *et al* [4].

Previous temperature dependent studies on iron borates $RFe_3(BO_3)_4$ using Moessbauer spectroscopy, specific heat, magnetic susceptibility or Raman spectroscopy revealed the existence of structural and magnetic phase transitions [5–7]. Without determining the actual low temperature nuclear space group or the magnetic structure, the work of Hinatsu *et al* [5] showed nicely that the transition temperatures of structural and magnetic transitions depend linearly on the ionic size of the rare earth ion. A structural phase transition from $R32$ to the slightly less symmetric $P3_121$ space group was first determined for $GdFe_3(BO_3)_4$ to occur at about 160 K by Klimin *et al* [8]. Later on, the same transition to $P3_121$ was found to occur as well in the equivalent Y (445 K), Er (340 K) and Tb (240 K), compounds but not in $NdFe_3(BO_3)_4$ [7, 10]. The transition temperatures decrease strongly with increasing ionic radius of the rare earth, explaining why the too large radius of Nd^{3+} prevents the structural phase transition.

While the structural behaviour has been well studied by now, the discussion of the magnetic behaviour of the iron borates is strongly obscured by the lack of knowledge of the actual magnetic structures at low temperatures. Magnetic susceptibility data determined the temperatures of the magnetic transitions to vary between about 40 K for the Tb compound and about 23 K for the La compound [5]. It was again possible to establish a linear relationship to the ionic size of the R^{3+} ion. Detailed data on the Gd and the Nd compounds revealed for these two compounds a second magnetic transition at even lower temperatures absent in the Y and the La compounds.

The combination of a strongly anisotropic nuclear structure with the presence of highly anisotropic magnetic rare earth ions characterizes these compounds, and it was suspected to be at the origin of a magnetic behaviour dominated by polarization and spin reorientation phenomena. This is the reason why the first suggestion of the magnetic structure of the Nd compound believed the iron sublattice to have only 1D correlations below 35 K and three-dimensional long range order of both the iron and the Nd sublattice only below 6 K [4]. For the Gd compound it was first thought that the magnetic transition at 37 K affected only the iron sublattice, leading to its long range order, while the second transition of 9 K was interpreted as a spin reorientation of the iron spins, with the Gd sublattice remaining paramagnetic down to the lowest temperatures [6]. Only recently, a simultaneous ordering of both sublattices was proposed [9] and confirmed [10] for the Nd, while for the Gd compound the rare earth sublattice magnetic order was thought to set in at about 20 K as the result of a strong polarization from the iron–rare earth exchange interaction [11]. Pankrats *et al* [11] proposed from their magnetic resonance data that in $GdFe_3(BO_3)_4$ the iron sublattice sees below 38 K an antiferromagnetic ordering with the spin direction within the *a–b*-plane before the strong influence of the anisotropy of the Gd sublattice leads at 10 K to a spin reorientation, which results in a magnetic structure where both sublattices form ferromagnetically aligned *a–b*-planes, which are ordered antiferromagnetically along the *c*-axis. Klimin *et al* [8] pointed out that the reduction in nuclear symmetry from $R32$ to $P3_121$ as found in $GdFe_3(BO_3)_4$ leads to two non-equivalent Fe sites and that this non-equivalence should be taken into account when interpreting the magnetic properties.

The fact that all the information on the magnetic structure in the $RFe_3(BO_3)_4$ compounds was coming from macroscopic measurements motivated our study on $TbFe_3(BO_3)_4$ using the microscopic method of neutron diffraction. The Tb compound was chosen as the starting point of a more general study, as Tb is not strongly absorbing (like e.g. Gd, Eu and Dy) and possesses normally a rather big magnetic moment, easily seen in magnetic neutron diffraction.

2. Experimental details

2.1. Sample preparation

Because of the strong neutron absorption of natural boron, samples with ^{11}B enriched to 99% were prepared at Krasnoyarsk. The $TbFe_3(^{11}BO_3)_4$ single crystals were grown from flux of 75 mass % $(Bi_2Mo_3O_{12} + 2, 5^{11}B_2O_3 + 0, 5Tb_2O_3) + 25$ mass % $TbFe_3(^{11}BO_3)_4$ [12]. The saturation temperature was $T_s \approx 950\,°C$, and the concentration (n) dependence of T_s had been $dT_s/dn = 5\,°C/mass\,\%$. The flux with mass of 150 g was prepared by melting at the temperature of $1100\,°C$ Bi_2O_3, MoO_3, $^{11}B_2O_3$, Fe_2O_3 and Tb_2O_3 oxides, using a platinum crucible. At this temperature the flux was kept for 4 h for homogenization. Afterwards the flux temperature was lowered to $T = T_s + 5\,°C$, the platinum rod with four seeds was settled down into the flux and a rotation of 30 revolutions per minute of the rod was switched on. After 15 min the flux temperature was lowered to $T = T_s - 7\,°C$. Then the temperature was reduced by $(1–2)\,°C/24$ h. The total duration of the crystal growth was about 18 days. Crystals with linear dimensions up to 15 mm were grown. Powder was prepared from these crystals by grinding.

2.2. Magnetization and neutron diffraction measurements

The magnetization measurements were carried out by the current shell method on the vibration magnetometer with a superconducting solenoid between 1.5 and 300 K and magnetic fields up to 80 kOe. The crystal was fixed on the quartz mount with its orientation controlled by the natural facet pattern with $\sim 2°$ accuracy. The total measurement error including magnetization, field, temperature and mass of the sample does not exceed $\sim 4\%$.

Neutron diffraction data were taken at the Institut Laue Langevin in Grenoble, France, on the high resolution powder diffractometer D1A and the high intensity powder diffractometer D1B. The temperature dependence of the diffraction pattern was measured using scans of 10 min between 3 and 300 K on D1B ($\lambda = 2.52$ Å) with a temperature resolution of 1 K up to 50 K and of 4 K between 50 and 300 K. Individual data points with greatly increased statistics (4 h) were taken as well at 2, 18, 27 and 50 K in order to reveal small details of the spectrum better. The high resolution data on D1A ($\lambda = 1.91$ Å) were taken at 2, 30, 40, 50, 100, 200 and 300 K. The absence of any impurity peaks as well as the narrowness of the neutron diffraction lines confirmed the compound to be single phase and well crystallized.

3. Results and discussion

Figure 1(a) shows the susceptibility data taken with the external magnetic field $H = 1$ kOe applied parallel and perpendicular to the crystal axis c. While no anomaly is seen with $H \perp c$, a sharp cusp at about 40 K can be seen in the $H \parallel c$ data. Closer inspection of this curve reveals a further anomaly slightly below the cusp at about 35 K. The parallel susceptibility $\chi_\parallel$ goes to zero at $T \rightarrow 0$ but there is a small anomaly at $T = 2$ K probably connected to an intrinsic Tb subsystem ordering due to dipole–dipole interactions or due to indirect Tb–Tb interactions via the non-magnetic BO_3 groups. In the temperature range $200\,K < T < 300\,K$ the inverse parallel susceptibility $\chi_\parallel^{-1}$ follows a Curie–Weiss law with the parameters $\theta_\parallel = 50$ K and $\mu_{eff} = 13.25\,\mu_B$ per formula unit. Assuming $\mu_{eff\,Fe} = 5.92\,\mu_B$ for the Fe^{3+} (S state ion) the effective magnetic moment for Tb was obtained, $\mu_{eff\,Tb} = 8.39\,\mu_B$. The perpendicular susceptibility $\chi_\perp$ is one-eighth of $\chi_\parallel$ and practically does not depend on temperature. Such a behaviour at $H \perp c$, especially at low temperatures, is determined by

3

(a)

(b)
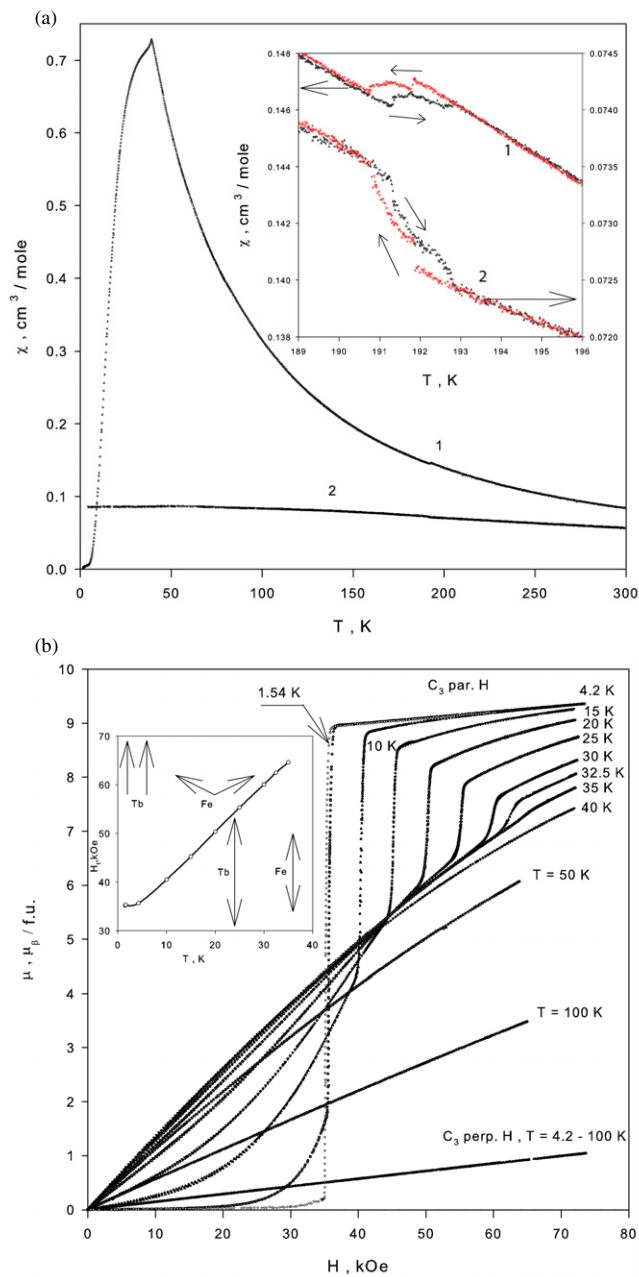
Figure 1. (a) The molar susceptibility of the $TbFe_3(BO_3)_4$ single crystal. 1, $H \parallel c$; 2, $H \perp c$. Inset: temperature range in the vicinity of the structural phase transition. Large arrows indicate the Y scale, small arrows the sense of the temperature variation. (b) Magnetization isotherms of the $TbFe_3(BO_3)_4$ single crystal for different orientations. Inset: the phase diagram H_t versus T.

strongly anisotropic g-values with g_a and g_b approaching zero. The magnetization process is determined by the temperature independent Van Vleck paramagnetism term. The inverse perpendicular susceptibility $\chi_\perp^{-1}$ does not follow the Curie–Weiss law at high temperatures.

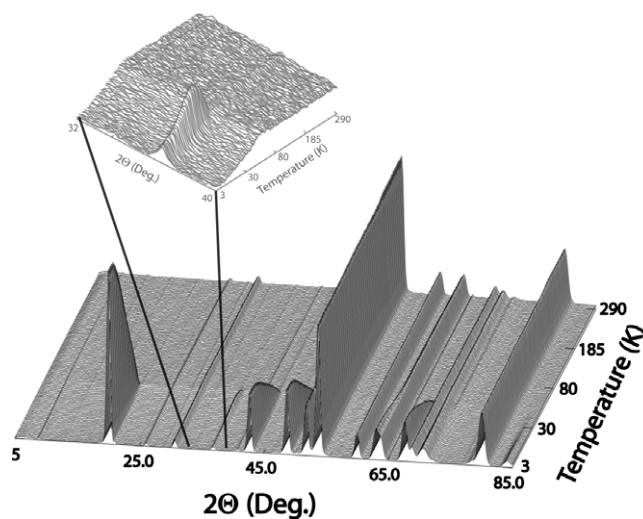**Figure 2.** Thermal dependence of the neutron diffraction pattern (thermodiffractogram) of TbFe$_3$(BO$_3$)$_4$. The inset shows an enlarged view of a magnetic peak displaying a decrease of intensity on cooling.

Any remarkable anisotropy in the a–b-plane is absent. Hysteresis anomalies in $\chi_\parallel$ and $\chi_\perp$ are found at $T = 192$ K (inset of figure 1(a)), which reflect the first order structural phase transition confirmed by the neutron data (see below).

In figure 1(b) the magnetization isotherms are presented for different temperatures and orientations of the external magnetic field. The demagnetization factor was taken into account. A sharp rise of the magnetization was obtained with $H \parallel c$ at $H_t = 35$ kOe $< H < 60$ kOe for different temperatures. The phase diagram H_t versus T is shown in the inset of figure 1(b). The largest value of the magnetization jump occurs at the lowest temperature and amounts to 9 μ_B, a value which corresponds closely to the Tb magnetic moment value. Therefore, we can say that the magnetization measurements confirm the existence of a metamagnetic transition in the Tb sublattice of the TbFe$_3$(BO$_3$)$_4$ crystal. The possible magnetic spin structures below and above H_t are shown in the inset of figure 1(b). It seems reasonable to assume that the critical field H_t needed to induce the metamagnetic transition corresponds to the value of the Fe sublattice exchange field acting on the Tb sublattice.

From the experimental data for $H > H_t$ and $T = 1.6$–4.2 K (figure 1(b)) neglecting the Tb sublattice paraprocess the value of the exchange field inside the Fe sublattice may be evaluated from the extrapolation of the linear dependence of the magnetization to the theoretical saturation magnetization of 24 μ_B as $2H_E = 1410$ kOe. Analogous measurements on a YFe$_3$(BO$_3$)$_4$ crystal (unpublished results) revealed an effective exchange field equal to $2H_E(\text{YFe}_3(\text{BO}_3)_4) = 1400$ kOe. The very good agreement of these two values confirms our argumentation on the exchange field nature in TbFe$_3$(BO$_3$)$_4$.

The magnetization curves are linear for the field applied parallel to the a–b-plane and do not depend on T for 4.2 K $< T < 100$ K in accordance with the temperature dependence of $\chi_\perp$. The magnetization has no anisotropy within the a–b-plane. The estimation of the saturation field for $H \perp c$ gives $H_{S\perp} = 1710$ kOe. So, the anisotropy field of the terbium iron borate can be estimated as $H_A = H_{S\perp} - 2H_E \approx 300$ kOe.

In figure 2 we show the thermodiffractogram measured on D1B. Clearly seen can be the appearance of additional Bragg peaks at low temperatures, which indicate the arising of strong
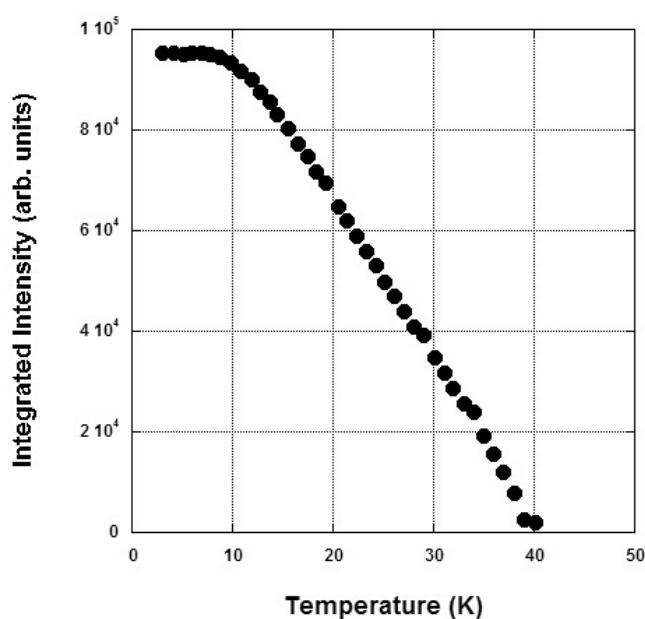
Figure 3. Integrated intensity of the $(0, 1, \frac{1}{2}/1, 0, \frac{1}{2})$ magnetic peak as a function of temperature.

long range ordered magnetism. Plotting the integrated intensity of the strongest new peak, which appears at about $2\Theta = 20°$, a magnetic transition temperature of about 40 K can be deduced (figure 3). This is in accordance with the transition temperatures determined by Hinatsu *et al* [5] and our own susceptibility data. The inset of figure 2 shows an enlargement of parts of the thermodiffractogram in a region with a magnetic peak showing a distinctly different behaviour. Figure 4 shows the integrated intensity of this peak: following an appearance at again about 40 K the intensity passes through a maximum at about 30 K before decreasing strongly down to the lowest temperatures. This behaviour can be typically found in magnetic systems which possess two magnetic sublattices showing different temperature dependences. In the case of $TbFe_3(BO_3)_4$ the two sublattices should be associated with the Fe and the Tb sublattice. The fact that the magnetic scattering is strongly visible still at quite high 2Θ values (e.g. the peak at 84° in figure 2) is a further indication of the presence of a long range ordered Tb sublattice, as—in contrast to the Fe magnetic form factor—the magnetic form factor of terbium does not fall off very rapidly with 2Θ.

No clear indication for a structural phase transition can be found in the thermodiffractogram at higher temperatures. However, a slight systematic shift of the Bragg peak positions and a slight change of intensity of some peaks can be found at around 200 K. Figure 5(a) displays the integrated intensity of the peak at 63.6°, which corresponds to the $(2, 2, 0)$ and $(1, 2, 2)$ peaks within the $R32$ space group, while figure 5(b) displays the peak position of the $(2, 1, 1)$ peak. One can conclude from the high intensity data that there are clear indications for one low temperature transition at about 40 K, one further anomaly at 30 K and the indication of a possible structural transition at 200 K.

The high resolution data at 300 K are shown in figure 6(a). Using the Rietveld refinement programme FULLPROF [14] the data can be refined in the expected space group $R32$, table 1 gives the result of the refinement and the most important bond lengths. Included as well are the results of the 200 K data, which can also be refined in space group $R32$. This is no longer
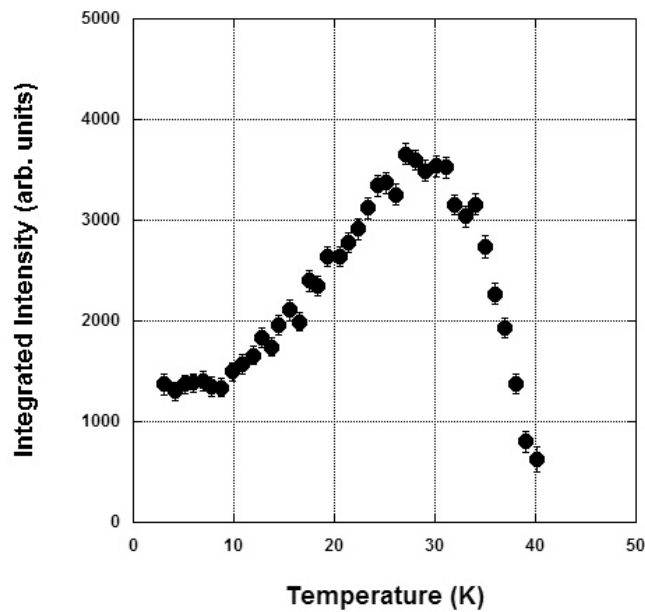
Figure 4. Integrated intensity of the $(2, 0, \frac{1}{2}/0, 2, \frac{1}{2})$ magnetic peak as a function of temperature.

possible for the high resolution data at lower temperatures: small additional structural peaks appear and the peak intensities do also differ slightly from the high temperature situation. As already indicated by the high intensity data, the high resolution data now show clearly that a structural phase transition to a less symmetric space group takes place below 200 K. The refinement proceeds smoothly using the space group $P3_121$, which had been determined by Klimin *et al* [8] for the similar compound $GdFe_3(BO_3)_4$ at low temperatures (figure 6(b)). Table 2 shows the results of the nuclear refinements using $P3_121$ of the high resolution data for $T < 200$ K. Listed are also again the most important bond distances and bond angles. The numbering of the atoms follows the numbering used by Klimin *et al* [8] in order to facilitate any comparison.

For the refinement of the high resolution data with $T < 40$ K, the presence of magnetic peaks has to be taken into account. The magnetic structure and therefore the magnetic symmetry are, however, unknown and have to be determined either by trial and error or by magnetic symmetry analysis [13]. The magnetic Bragg peaks can be indexed using a nuclear unit cell doubled in the c-direction; the magnetic propagation vector is therefore $k = [0, 0, \frac{1}{2}]$ and we can conclude that the magnetic structure is antiferromagnetic and commensurate with the nuclear lattice. The presence of three possible magnetic ions (two iron and one terbium) in the nuclear unit cell prompted us to use magnetic symmetry analysis for the determination of the allowed irreducible representations of $k = [0, 0, \frac{1}{2}]$ in space group $P3_121$. Magnetic symmetry analysis is no longer tedious, as nowadays computer programs are available which demand as input information solely the nuclear space group, the propagation vector and the position of the independent magnetic ions. We used the two independent programs Basisreps [14] and Sarah [15], which both calculated the existence of three irreducible representations for our special case. Both programs provide the user with the possibility to extract command lines for the magnetic refinement for use in the refinement program FULLPROF [14]. Trying out these three possible solutions it turned out that a one-dimensional representation with

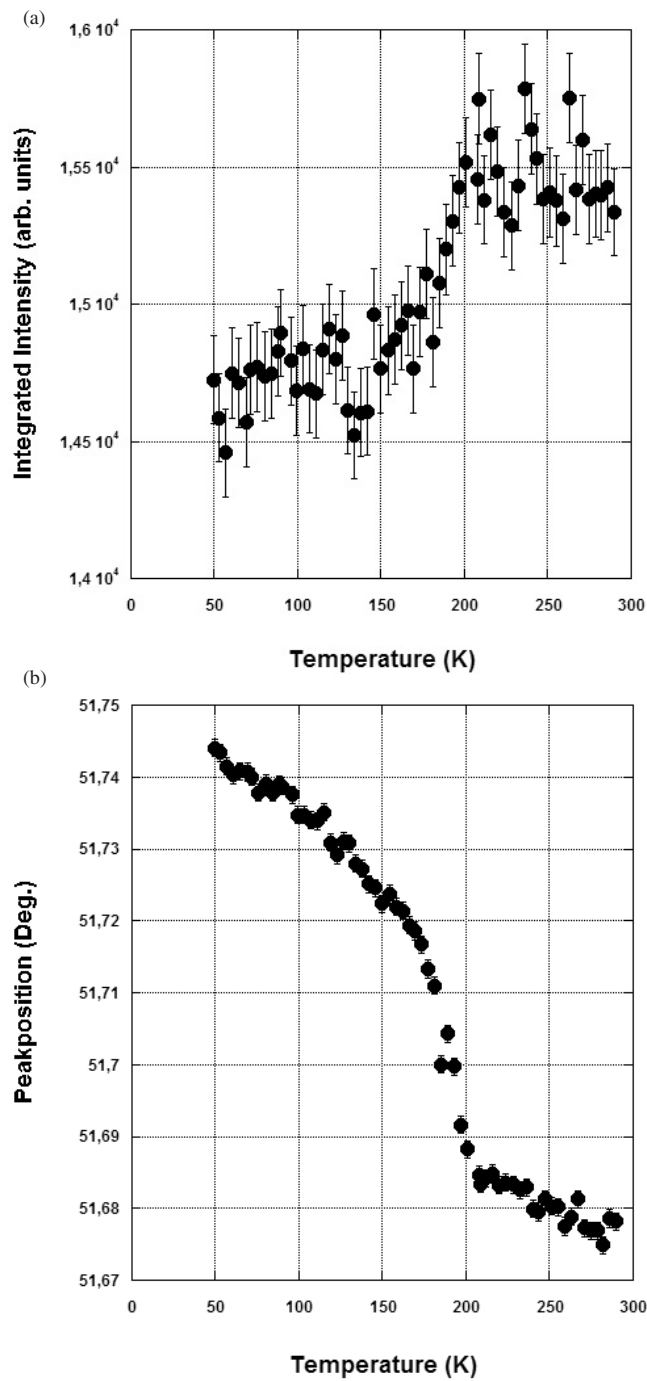**Figure 5.** (a) Integrated intensity of the nuclear (2, 2, 0/1, 2, 2) peak as a function of temperature. (b) Angular position of the nuclear (2, 1, 1) Bragg peak as a function of temperature.

respectively two, three and two basis functions for the Fe1, Fe2 and Tb sites provides the correct description of the magnetic structure. A first refinement of the high resolution data
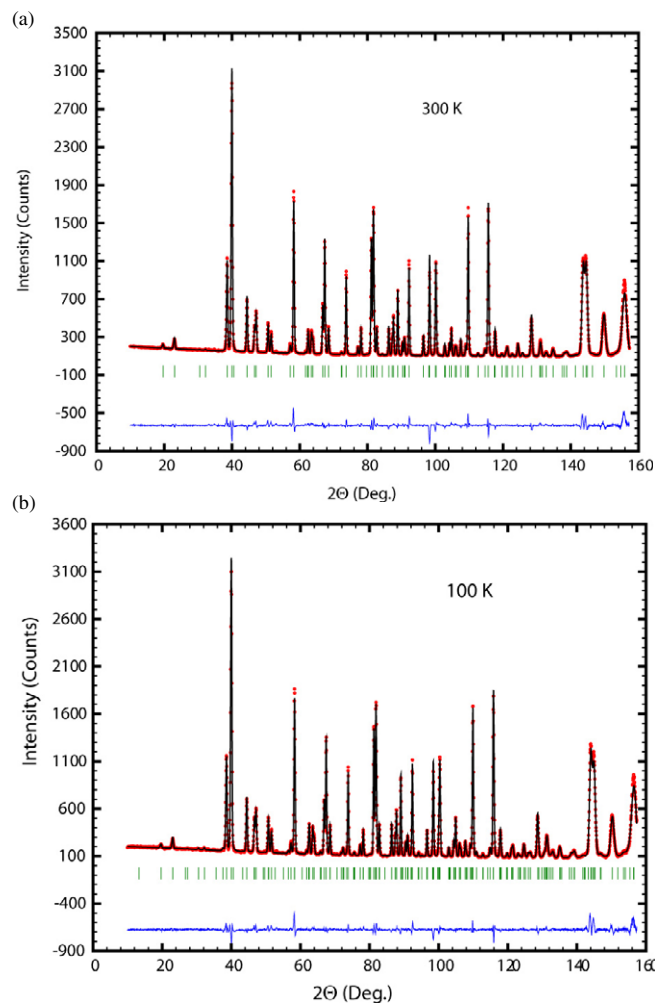
(a)

(b)

Figure 6. (a) Observed (dots, red), calculated (line, black) and difference pattern of TbFe$_3$(BO$_3$)$_4$ at 300 K refined in R32. The tick marks indicate the calculated position of the Bragg peaks. (b) Observed (dots, red), calculated (line, black) and difference pattern of TbFe$_3$(BO$_3$)$_4$ at 100 K refined in $P3_1$21. The tick marks indicate the calculated position of the Bragg peaks.

which let the magnetic moment values of the two iron sites vary freely resulted for the 2 K data in values of 4.0(3) μ_B for the Fe1, 4.4(2) μ_B for the Fe2 sites and 8.54(6) μ_B for the Tb site. The difference between the moment values of the two iron sites seems at first to be significant and could point to a different valence of the two sites. However, bond valence calculations (done by the program FULLPROF using the structural details given in table 2) resulted in a valence of about $+3$ for both sites and therefore gave no indication in this direction. The only difference between the two iron sites resides in the Fe–Fe distances, which are insignificantly longer in case of the Fe2 sites (table 2). A closer look at the refinement revealed that the moment values of the two sites were strongly correlated in the refinement—leading also to large values of the errors—and it was therefore decided to constrain them to have the same moment value. This reduced strongly the error connected to the so determined iron moment of $\mu_{Fe} = 4.39(4)$ μ_B while the terbium moment $\mu_{Tb} = 8.53(5)$ μ_B remained

Table 1. Structural data of $TbFe_3(BO_3)_4$ at 300 and 200 K refined in space group $R32$. Important inter-atomic distances and angles.

|	300 K	200 K
a (Å)	9.552 36(7)	9.550 50(7)
c (Å)	7.573 70(8)	7.568 43(8)
Tb (3a): x	0	0
y	0	0
z	0	0
Fe (9d): x	0.5493(1)	0.5493(1)
y	0	0
z	0	0
O1 (9e): x	0.8542(3)	0.8542(3)
y	0	0
z	1/2	1/2
O2 (9e): x	0.5924(2)	0.5927(2)
y	0	0
z	1/2	1/2
O3 (18f) x	0.0240(1)	0.0239(2)
y	0.2111(1)	0.2110(2)
z	0.1838(2)	0.1839(2)
B1 (3b) x	0	0
y	0	0
z	1/2	1/2
B2 (9e) x	0.4475(2)	0.4478(2)
y	0	0
z	1/2	1/2
$6 \times$ Tb–O3 (Å)	2.365(1)	2.365(1)
$2 \times$ Fe–O1 (Å)	2.013(2)	2.012(2)
$2 \times$ Fe–O2 (Å)	2.037(2)	2.034(2)
$2 \times$ Fe–O3 (Å)	1.967(2)	1.967(1)
Fe–Fe (Å)	3.1848(9)	3.1830(9)
Fe–O1–Fe (deg)	104.5(1)	104.6(1)
Fe–O2–Fe (deg)	102.9(1)	103.0(1)
Tb–O3–Fe (deg)	120.6(1)	120.6(1)

unchanged. Figure 7 shows the refined data at 2 K; figure 8 displays the model of the magnetic structure of $TbFe_3(BO_3)_4$. Iron and terbium spins are antiferromagnetically coupled along the c-direction; the moments also point along c. It can be seen nicely in figure 8 how the antiferromagnetic coupling between the Fe spins is transmitted along the one-dimensional structure element of the helicoidal chains of Fe^{3+} ions. This antiferromagnetic intrachain coupling proceeds either through direct Fe–Fe exchange or through Fe–O–Fe superexchange (see figure 4 of [8]). The Fe–O–Fe bond angles for this superexchange are in the range $102.4°$–$105.5°$ (table 2). Within the a–b-planes all Fe spins possess the same direction while the Tb spins are antiferromagnetically aligned to them. Klimin *et al* [8] suggested that the interchain interactions should be transmitted mainly through Fe–O–O–Fe exchange and less importantly through superexchange involving the magnetic rare earth. In the case of $TbFe_3(BO_3)_4$ every Fe spin is interacting with one Fe spin of four neighbouring helicoidal chains within the same a–b-plane through two Fe–O–O–Fe superexchange pathways. This exchange is ferromagnetic with the two interacting Fe spins being arranged in *cis* configuration with respect to two different connecting O–O exchange paths (figure 9, exchange 1–2 and 4–

Table 2. Structural data of TbFe$_3$(BO$_3$)$_4$ at 100, 40, 30 and 2 K refined in space group $P3_121$. Important inter-atomic distances and angles.

	2 K	30 K	40 K	100 K
a (Å)	9.536 77(11)	9.538 65(9)	9.539 75(7)	9.541 64(6)
c (Å)	7.566 48(12)	7.567 37(10)	7.567 18(8)	7.565 87(7)
Tb (3a) x	0.666(1)	0.665(1)	0.6658(8)	0.6660(8)
y	0.666(1)	0.665(1)	0.6658(8)	0.6660(8)
z	0	0	0	0
Fe1 (3a) x	0.117(1)	0.1161(8)	0.1164(6)	0.1163(6)
y	0.117(1)	0.1161(8)	0.1164(6)	0.1163(6)
z	0	0	0	0
Fe2 (6c) x	0.7858(7)	0.7863(6)	0.7863(5)	0.7857(5)
y	0.4497(7)	0.4503(5)	0.4505(4)	0.4501(4)
z	0.3414(6)	0.3417(5)	0.3418(4)	0.3415(4)
O1 (3b) x	0	0	0	0
y	0.925(2)	0.925(1)	0.925(1)	0.925(1)
z	1/6	1/6	1/6	1/6
O2 (6c) x	0.416(1)	0.417(1)	0.4168(8)	0.4165(8)
y	0.727(1)	0.727(1)	0.7273(7)	0.7283(7)
z	0.1313(8)	0.1320(6)	0.1330(5)	0.1345(5)
O3 (6c) x	0.875(1)	0.876(1)	0.8758(8)	0.8762(8)
y	0.694(1)	0.695(1)	0.6935(9)	0.6933(9)
z	0.822(1)	0.822(1)	0.8225(8)	0.8215(8)
O4 (6c) x	0.855(1)	0.856(1)	0.8554(9)	0.8563(9)
y	0.640(1)	0.642(1)	0.6412(9)	0.6414(9)
z	0.186(1)	0.185(1)	0.1849(8)	0.1857(8)
O5 (6c) x	0.477(1)	0.4772(9)	0.4762(6)	0.4772(7)
y	0.142(1)	0.142(1)	0.1433(9)	0.1424(9)
z	0.841(1)	0.841(1)	0.8426(8)	0.8415(8)
O6 (3b) x	0.185(2)	0.185(1)	0.185(1)	0.1856(1)
y	0	0	0	0
z	5/6	5/6	5/6	5/6
O7 (6c) x	0.475(1)	0.4755(9)	0.4765(7)	0.4759(7)
y	0.462(1)	0.461(1)	0.4603(9)	0.4589(9)
z	0.815(1)	0.8143(9)	0.8129(7)	0.8146(7)
B1 (3b) x	0.332(2)	0.331(1)	0.332(1)	0.331(1)
y	0	0	0	0
z	5/6	5/6	5/6	5/6
B2 (6c) x	0.550(1)	0.550(1)	0.5517(8)	0.5514(8)
y	0.880(1)	0.8808(8)	0.8805(6)	0.8818(6)
z	0.149(1)	0.1491(8)	0.1503(6)	0.1508(6)
B3 (3b) x	0	0	0	0
y	0.780(1)	0.780(1)	0.780(1)	0.781(1)
z	1/6	1/6	1/6	1/6
$2 \times$ Tb–O3 (Å)	2.31(1)	2.32(1)	2.315(9)	2.322(9)
$2 \times$ Tb–O4 (Å)	2.40(1)	2.39(1)	2.39(1)	2.38(1)
$2 \times$ Tb–O7 (Å)	2.35(1)	2.349(9)	2.360(7)	2.362(7)
$2 \times$ Fe1–O1 (Å)	2.037(6)	2.028(10)	2.031(7)	2.032(8)
$2 \times$ Fe1–O3 (Å)	1.979(15)	1.973(11)	1.984(8)	1.980(8)
$2 \times$ Fe1–O6 (Å)	1.995(13)	1.997(11)	1.996(8)	1.999(8)
Fe2–O2 (Å)	2.008(10)	2.022(8)	2.024(6)	2.021(6)
Fe2–O2 (Å)	2.069(10)	2.069(8)	2.067(6)	2.064(6)
Fe2–O4 (Å)	1.982(13)	1.991(10)	1.989(8)	1.989(8)
Fe2–O5 (Å)	2.010(15)	2.005(12)	2.010(9)	2.006(9)

Table 2. (Continued.)

	2 K	30 K	40 K	100 K
Fe2–O5 (Å)	2.051(15)	2.051(12)	2.045(9)	2.047(9)
Fe2–O7 (Å)	1.986(11)	1.970(9)	1.952(7)	1.957(7)
Fe1–Fe1 (Å)	3.175(7)	3.169(6)	3.172(4)	3.171(4)
Fe2–Fe2 (Å)	3.185(7)	3.191(6)	3.192(5)	3.187(5)
Tb–O3–Fe1 (deg)	122.8(7)	123.0(6)	122.5(4)	122.2(4)
Tb–O4–Fe2 (deg)	121.2(8)	120.9(7)	121.2(5)	121.4(5)
Tb–O7–Fe2 (deg)	117.1(7)	117.4(6)	117.9(4)	117.8(4)
Fe1–O1–Fe1 (deg)	102.4(6)	102.7(5)	102.7(4)	102.5(4)
Fe1–O6–Fe1 (deg)	105.5(7)	105.5(5)	105.2(4)	105.0(4)
Fe2–O2–Fe2 (deg)	102.8(6)	102.5(5)	102.6(4)	102.6(4)
Fe2–O5–Fe2 (deg)	103.3(6)	103.8(5)	103.9(4)	103.7(4)
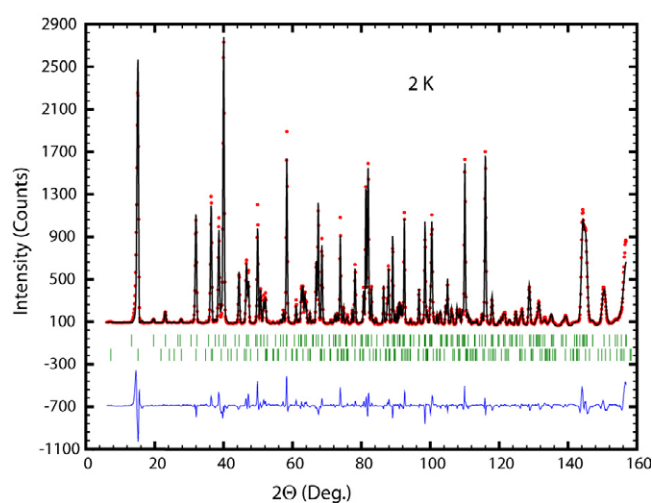
Figure 7. Observed (dots, red), calculated (line, black) and difference pattern of $TbFe_3(BO_3)_4$ at 2 K refined in $P3_121$. The tick marks indicate the calculated position of the nuclear (upper row) and magnetic (lower row) Bragg peaks.

3). A second Fe–O–O–Fe superexchange, but this time with the iron spins being arranged in *trans* configuration and antiferromagnetic (figure 9, exchange 1–3), exists to one iron spin of each of the six surrounding chains, these iron spins lying in the *a–b*-planes above or below. Furthermore there are two antiferromagnetic Fe–O–O–Fe exchange paths to two iron spins of the nearest two chains forming a *cis* configuration (figure 9, exchange 4–2). This means that the magnetic interaction of every Fe spin to the neighbouring helicoidal chains is determined by $4 \times 2 = 8$ ferromagnetic and $6 + 2 = 8$ antiferromagnetic Fe–O–O–Fe superexchange pathways of similar length but different configurations. It can be expected that due to the multitude and the nonsymmetric nature of the different pathways slight changes in the overall interatomic distances will lead to changes in the magnetic structure of the Fe sublattice. The strength of this interchain interaction is e.g. certainly dependent on the distance between the two connecting oxygen atoms which is already quite large in $TbFe_3(BO_3)_4$ at 2.3–2.4 Å.

Figure 10 shows part of the magnetic unit cell highlighting the Fe–O–Tb–O–Fe superexchange. It comprises only ferromagnetic interactions and is highly symmetric: there
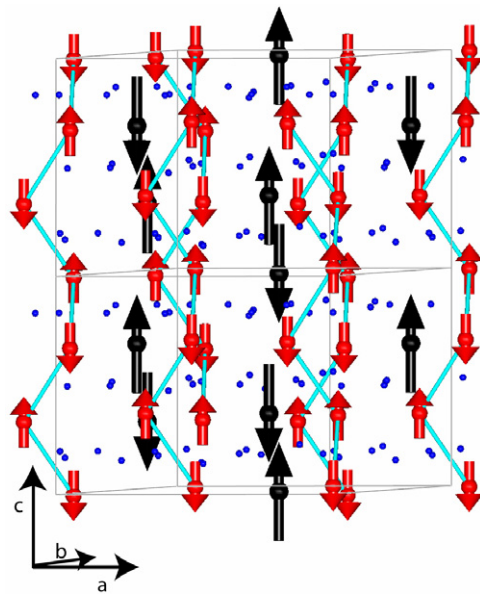
Figure 8. Magnetic structure of $TbFe_3(BO_3)_4$. Tb spins in black, Fe spins in grey (red), the direct Fe–Fe exchange along the helicoidal chains is indicated by light grey (blue) lines. The position of the oxygen atoms is represented by small black (blue) spheres; boron atoms are omitted for clarity.
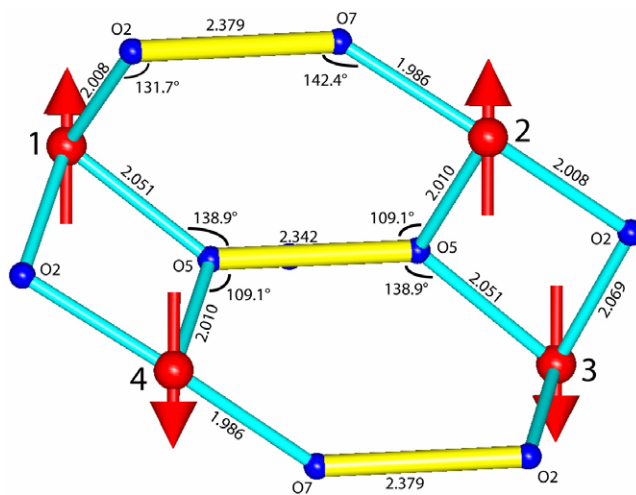

Figure 9. Structural details of the antiferromagnetic intrachain Fe–O–Fe interaction (Fe1–Fe4, Fe2–Fe3) and of the different interchain ferromagnetic (Fe1–Fe2, Fe4–Fe3) and antiferromagnetic (Fe1–Fe3, Fe4–Fe2) exchange paths. Iron spins in black (red), oxygen atoms represented by small black (blue) spheres. Bond lengths and bond angles given are those for the case of the two neighbouring chains consisting of Fe2 sites. In the case of two neighbouring chains being formed by Fe1 sites and Fe2 sites the same intrachain and interchain interactions exist with very similar bond lengths (see table 2).

are no interactions between the Fe and the Tb sublattices within one *a*–*b*-plane but every Tb spin sees six ferromagnetic interactions with three Fe spins lying in the *a*–*b*-plane above
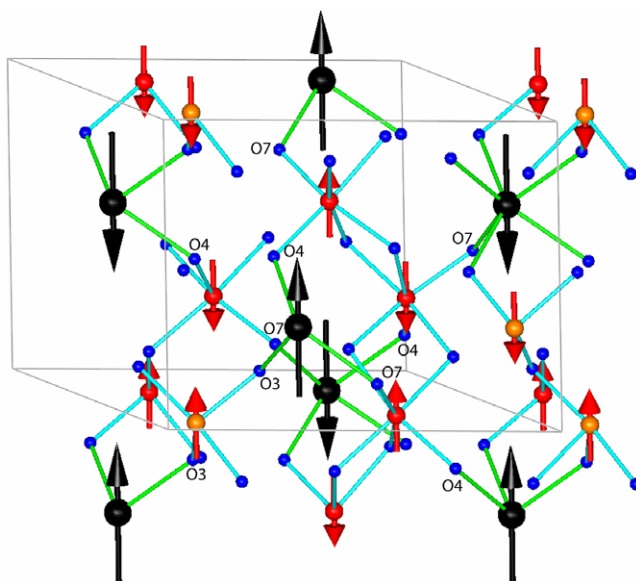
13

Figure 10. The exclusively ferromagnetic Tb–O4–Fe2–O7–Tb and Tb–O3–Fe1–O3–Tb superexchange interactions. Tb spins in black, Fe spins in grey (red), oxygen atoms as small black (blue) spheres. Fe1 atoms in medium size light grey (orange) spheres, Fe2 atoms in medium size dark grey (red) spheres.

and to three Fe spins lying in the a–b-plane below. Due to the two different iron sites there are two different exchange paths (Tb–O4–Fe2–O7–Tb and Tb–O3–Fe1–O3–Tb, see figure 10), which differ, however, only slightly in the bond distances and bond angles involved (table 2). It can be speculated that this symmetric, three-dimensional network of exchange paths between the Tb and the Fe sublattices is contributing significantly to the formation and the stabilization of the overall magnetic structure and to the surprisingly high T_N of TbFe$_3$(BO$_3$)$_4$. This microscopically determined magnetic structure of TbFe$_3$(BO$_3$)$_4$ is not too different from the structure proposed by Pankrats *et al* [11] for GdFe$_3$(BO$_3$)$_4$: they also see the antiferromagnetic alignment of Fe and rare earth spins along c with the spin direction in c but suppose all sublattices to possess parallel spin directions within one a–b-plane leading to an antiferromagnetic alignment between the rare earth and the iron spins along the R–O– Fe–O–R superexchange pathway. Comparing TbFe$_3$(BO$_3$)$_4$ to the magnetic structure found recently by Fischer *et al* [10] for NdFe$_3$(BO$_3$)$_4$, we have to notice that while the propagation vector is identical for the two compounds ($\kappa_{\text{hex}} = [0, 0, \frac{3}{2}]$ in the description using the R-centring corresponds to our $\kappa = [0, 0, \frac{1}{2}]$ for the primitive cell) the moment directions are completely different. While in the Tb compound the Fe and Tb sublattices are collinear and the spin direction is along the c-axis, in the Nd compound the spins all lie in the a–b-plane with a temperature dependent angle of 47°–77° between the two sublattices. As the structural differences between the two compounds are small apart from a volume increase of 1.7% when going from the Tb compound to the Nd compound, it is reasonable to assume that the fundamental differences in the spin directions are connected to the strong differences in the rare earth magnetic moment values (8.5 μ_B in TbFe$_3$(BO$_3$)$_4$ compared to 2.7 μ_B in NdFe$_3$(BO$_3$)$_4$) coupled to the strongly differing single ion anisotropies of the two 4f ions.

Having determined the magnetic structure of TbFe$_3$(BO$_3$)$_4$ in zero field it is tempting to interpret the metamagnetic transition found in the magnetization data with $H \parallel c$ as resulting
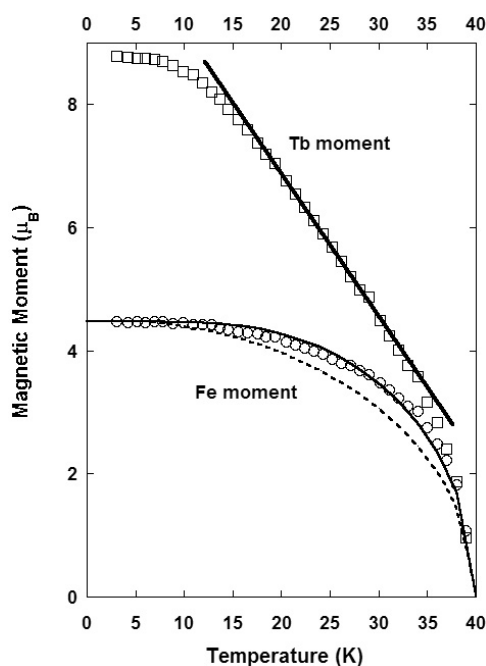
Figure 11. Temperature dependence of the magnetic moment values of the Tb sublattice (open squares) and the Fe sublattice (open circles). The dashed curve and the full curve are fits to the temperature dependence of the Fe magnetic moment with the Brillouin function using $J = 5/2$ and $J = \frac{1}{2}$ respectively. The straight line is a guide to the eye.

from the Tb sublattice adopting a purely ferromagnetic alignment parallel to the *c*-axis. Neutron diffraction data under a magnetic field are needed to ascertain this interpretation and to verify the possible occurrence of a spin-flop transition of the Fe spins.

A subsequent refinement of the high resolution data taken at 30 K resulted in magnetic moment values of 3.34(3) μ_B for Fe and 4.42(4) μ_B for Tb. The strong reduction of the terbium magnetic moment at 30 K compared to the 2 K value combined with the relatively small reduction of the iron moments indicates a different temperature dependence of the two magnetic sublattices. Using the structural parameters determined from the high resolution data at low temperatures and the known magnetic structure model, a refinement of the thermal dependence of the magnetic moment values was done on the high intensity data from D1B. Figure 11 displays the results of these refinements: the normal, Brillouin type behaviour of the Fe sublattice magnetization can be nicely seen while the Tb sublattice magnetization shows a nearly linear increase between 35 and 15 K. The onset of the long range ordering of the Tb sublattice sets in at exactly the same temperature ($T_N = 40$ K) as that of the Fe sublattice. It is not possible to fit the temperature dependence of the Fe sublattice magnetization to a Brillouin curve with $S = 5/2$. We argue that this is due to the additional excitation of the Fe sublattice by the Tb sublattice. In the same way, the Tb sublattice magnetization does not follow a Brillouin type curve as the magnetization process is not governed by a simple exchange interaction between Tb ions but is directly influenced by the magnetization of the Fe sublattice. The neutron diffraction data are very sensitive to the appearance of the Tb moment, as the intensity of the first strong magnetic peak $(0, 1, \frac{1}{2}/1, 0, \frac{1}{2})$ at $2\Theta = 15°$ is mostly determined by the contribution coming from the Tb sublattice. As the direct Tb–Tb interactions are too
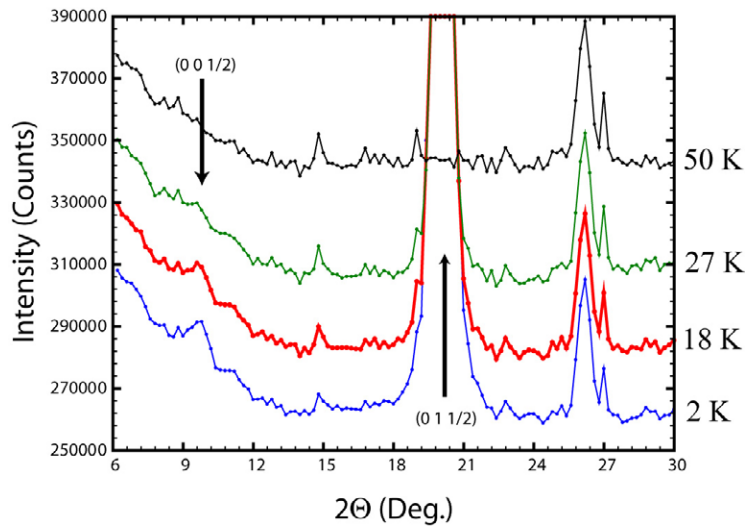
Figure 12. Part of the high intensity neutron diffraction data measured for 6 h per temperature point showing the existence of a small $(0, 0, \frac{1}{2})$ magnetic peak at low angles.

weak due to the isolated nature of the Tb ions within the lattice, we have to conclude that the appearance of the Fe magnetism induces by way of polarization long range magnetic order also on the Tb sublattice. Following a first strong increase just below T_N down to 35 K where the Fe moments reach about 65% of their saturation value the further increase of the Tb sublattice magnetization continues linearly and seems to be partly uncoupled from the Fe magnetism, which saturates at about 13 K. The change from pure polarization to long range magnetism of the Tb sublattice partly driven through Tb–O–Fe–O–Tb interactions (see above) must also be at the origin of the anomaly at about 30 K seen in the susceptibility data (figure 1(a)). We have to recall here that there are no significant changes in the interatomic distances or angles between 2, 30 and 40 K (table 2) which could play a role in the change of the magnetic interactions.

As mentioned above, data with strongly increased statistics were taken at selected temperatures below T_N. The reason for this was the fact that the irreducible representation, which describes the magnetic structure of $TbFe_3(BO_3)_4$, allows the existence of spin components not parallel to the c-direction. Figure 12 shows that there is indeed a tiny magnetic peak at the $(0, 0, \frac{1}{2})$ position: its intensity decreases as the temperature is increased but even at 27 K it is still discernible. The amount of spin canting off the c-direction cannot be determined reliably by a refinement due to the uniqueness of this characteristic peak and due to its very small intensity. It is therefore also not possible to determine directly whether all of the magnetic atoms contribute to the spin canting or just the Tb or the Fe sublattice. It is just possible to indicate an order of magnitude: the small intensity of the $(0, 0, \frac{1}{2})$ peak limits the spin moment values lying in the a–b-plane at 2 K to $\mu_{ab} \leqslant 0.5\ \mu_B$. The strong decrease of this component with increasing temperature between 18 and 27 K (figure 12) gives, however, the indication that it could be more related to the thermal behaviour of the Tb magnetic moment which at 27 K has reduced to about 60% of its low temperature value (figure 11). We have to recall here that the intensity of a magnetic Bragg peak is proportional to the square of the magnetic moment value so that a reduction of the magnetic moment value to 60% produces a magnetic Bragg peak of about one-third the intensity. This means that the small amount of spin canting off the c-direction reflected in the presence of the $(0, 0, \frac{1}{2})$ peak is not evolving suddenly but follows the thermal behaviour of the terbium magnetic moment value.

This means also that there is no indication whatsoever for a spin reorientation taking place in $TbFe_3(BO_3)_4$. This is in opposition to what was suggested for the equivalent Gd compound [11], where a first orientation of the Fe sublattice spin moments within the a–b-plane is thought to reorient to the c-direction under the growing influence of the anisotropy of the Gd sublattice.

4. Summary

Susceptibility and magnetization measurements on $TbFe_3(BO_3)_4$ reveal a strong anisotropic behaviour with the occurrence of a metamagnetic transition in an external magnetic field applied parallel to the c-axis. The values of the Fe sublattice exchange field and of the anisotropy field of the Tb rare earth ion are estimated. We have determined the nuclear and the magnetic structure of $TbFe_3(BO_3)_4$ as a function of temperature using neutron diffraction. A structural phase transition from $R32$ to $P3_121$ takes place at $T = 192$ K. An antiferromagnetic coupling along the helicoidal chains of Fe atoms with a magnetic propagation vector $\kappa = [0, 0, \frac{1}{2}]$ sets in at about 40 K. Within the a–b-planes of the structure all Fe spins are parallel but anti-parallel to the Tb spins, which are also antiferromagnetically ordered in the c-direction. At 2 K the magnetic moment values amount to about $\mu_{Fe} = 4.4 \ \mu_B$ and $\mu_{Tb} = 8.6 \ \mu_B$. Our study does confirm the polarization effect of the long-range ordered Fe sublattice on the Tb spins. The detailed analysis of the temperature dependence of the magnetic moments shows that this polarization leads in the case of the Tb compound to a magnetic moment induced immediately at T_N on the Tb site. Starting at about 35 K the indirect Tb–Tb interactions become important and lead to an increasing of the Tb sublattice magnetization, which is less coupled to the Fe sublattice magnetization. The symmetry reduction from $R32$ to $P3_121$ at high temperatures does not seem to have any important influence on the magnetic structure formed: the two inequivalent Fe-sites behave similarly, and for the magnetic coupling decisive bond lengths and bond angles are nearly identical. Bond valence calculations give a valence of about $+3$ for both Fe sites. The Fe–Fe distances within the two helicoidal chains along the c-direction are at Fe1–Fe1 = 3.170(6) Å and Fe2–Fe2 = 3.186(6) Å only different by 0.5%. Further studies on the related compounds $YFe_3(BO_3)_4$ and $HoFe_3(BO_3)_4$ are underway and will clarify further the role played by the rare earth sublattice and the interatomic bond distances.

References

[1] Brenier A, Tu C, Zhu Z and Wu B 2004 *Appl. Phys. Lett.* **84** 2034
[2] Zvezdin A K, Krotov S S, Kadomtseva A M, Vorob'ev G P, Popov Y F, Pytakov A P, Bezmaternykh L N and Popova E 2005 *JETP Lett.* **81** 272
[3] Joubert J C, White W and Roy R 1968 *J. Appl. Crystallogr.* **1** 318
[4] Campá J A, Cascales C, Gutiérrez-Puebla E, Monge M A, Rasines I and Ruíz-Valero C 1997 *Chem. Mater.* **9** 237
[5] Hinatsu Y, Doi Y, Ito K, Wakeshima M and Alemi A 2003 *J. Solid State Chem.* **172** 438
[6] Levitin R Z, Popova E A, Chtsherbov R M, Vasiliev A N, Popova M N, Chukalina E P, Klimin S A, van Loosdrecht P H M, Fausti D and Bezmaternykh L N 2004 *JETP Lett.* **79** 423
[7] Fausti D, Nugroho A A, van Loosdrecht P H M, Klimin S A, Popova M N and Bezmaternykh L N 2006 *Phys. Rev.* B **74** 024403
[8] Klimin S A, Fausti D, Meetsma A, Bezmaternykh L N, van Loosdrecht P H M and Palstra T T M 2005 *Acta Crystallogr.* B **61** 481
[9] Chukalina E P, Kuritsin D Y, Popova M N, Bezmaternykh L N, Kharlamova S A and Temerov V L 2004 *Phys. Lett.* A **322** 239
[10] Fischer P, Pomjakushin V, Sheptyakov D, Keller L, Janoschek M, Roessli B, Schefer J, Petrakovskii G A, Bezmaternikh L N, Temerov V and Velikanov D 2006 *J. Phys.: Condens. Matter* **18** 7975
[11] Pankrats A I, Petrakovskii G A, Bezmaternykh L N and Bayukov O A 2004 *JETP* **99** 766
[12] Bezmaternykh L N, Kharlamova S A and Temerov V L 2004 *Krystallografiya* **49** 945
[13] Bertaut E F 1968 *Acta Crystallogr.* A **24** 217
[14] Rodríguez-Carvajal J 1993 *Physica* B **192** 55
[15] Wills A S 2000 *Physica* B **276–278** 680